

Direct Assembly of Hydrophobic Nanoparticles to Multifunctional Structures

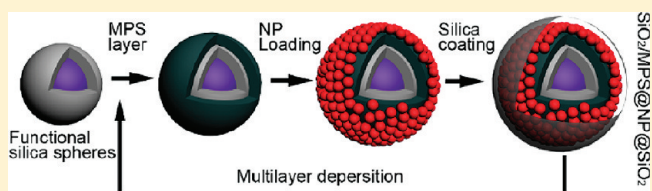
Zhenda Lu,[†] Chuanbo Gao,[†] Qiao Zhang,[†] Miaofang Chi,[‡] Jane Y. Howe,[‡] and Yadong Yin*,[†]

[†]Department of Chemistry, University of California, Riverside, California 92521, United States

[‡]Materials Science Division, Oak Ridge National Laboratory, Oak Ridge, Tennessee 37830, United States

 Supporting Information

ABSTRACT: We present a general process that allows convenient production of multifunctional composite particles by direct self-assembly of hydrophobic nanoparticles on host nanostructures containing high-density surface thiol groups. Hydrophobic nanoparticles of various compositions and combinations can be directly assembled onto the host surface through the strong coordination interactions between metal cations and thiol groups. The resulting structures can be further conveniently overcoated with a layer of normal silica to stabilize the assemblies and render them highly dispersible in water for biomedical applications. As the entire fabrication process does not involve complicated surface modification procedures, the hydrophobic ligands on the nanoparticles are not disturbed significantly so that they retain their original properties such as highly efficient luminescence. Many complex composite nanostructures with tailored functions can be efficiently produced by using this versatile approach. For example, multifunctional nonspherical nanostructures can be efficiently produced by using mercapto-silica coated nano-objects of arbitrary shapes as hosts for immobilizing functional nanoparticles. Multilayer structures can also be achieved by repeating the mercapto-silica coating and nanoparticle immobilization processes. Such assembly approach will provide the research community a highly versatile, configurable, scalable, and reproducible process for the preparation of various multifunctional structures.



KEYWORDS: Self-assembly, hydrophobic nanoparticles, multifunctional materials, mercapto-silica, multilayer structures

Multifunctional particles in the micrometer or submicrometer scale that exhibit two or more different properties are highly desirable for many important technological applications, ranging from catalysis to energy harvesting and transformation, multimodal imaging, detection, and simultaneous diagnosis and therapy.^{1–6} For example, microspheres embedded with magnetic iron oxide nanoparticles and fluorescent quantum dots have been widely studied as a multiple-mode imaging contrast agents combining magnetic resonance with optical detection and biological targeting.^{7–9} By carefully controlling the loading of quantum dots, the obtained composite particles possess a dual function of optical encoding and magnetic separation.^{6,10} Replacing quantum dots with noble metal nanoparticles in such composites results in new types of multifunctional structures that are capable of magnetic resonance imaging and photothermal therapy.^{11,12} Magnetic materials have also been combined with nanocatalysts to form magnetically separable catalysts for the recovery and reuse of expensive catalysts after catalytic reactions, thus bridging the gap between heterogeneous and homogeneous catalysis.^{13–16}

Nanoparticle assembly represents a powerful approach that has been actively explored recently for producing bi-, tri-, and multi-functional materials in contrast to their limited single-component counterparts. By organizing different types of nanoparticles together, it not only allows the utilization of the size- and shape-dependent properties of individual nanoparticles but also takes advantage of new properties resulting from the interactions between neighbors.^{2,3}

Conventional assembly processes for multifunctional structures such as the well-known layer-by-layer (LbL) methods are mostly limited to hydrophilic nanoparticle systems because they heavily rely on electrostatic interactions.^{17–19} The direct linking nanoparticles through chemical bonds between surface ligands has also been attempted^{20–22} but is limited to some special cases because most commonly used protecting ligands of nanoparticles do not contain additional active functional groups that allow further reactions.

Many technologically important high quality nanoparticles, especially semiconductors (such as CdSe, ZnSe, CdTe, and InP, InAs) and metal oxides (such as γ -Fe₂O₃, MnO, TiO₂, ZrO₂, CoFe₂O₄) are predominantly prepared through thermolytic routes by reacting inorganic precursors in organic solvents at high temperatures (typically 150–320 °C).^{23–27} The resulting nanostructures, however, retain the hydrophobic character of the organic ligands and, hence, are not soluble in water. As a result, it has been very difficult to assemble them directly into multifunctional nanostructures using means similar to those for water-soluble particles. Typically, it is necessary to impose hydrophilic character on the nanoparticle surface and ensure water dispersibility (also biocompatibility) by replacing the hydrophobic organic ligands with hydrophilic ones.^{28–30} However, ligand

Received: May 29, 2011

Revised: June 23, 2011

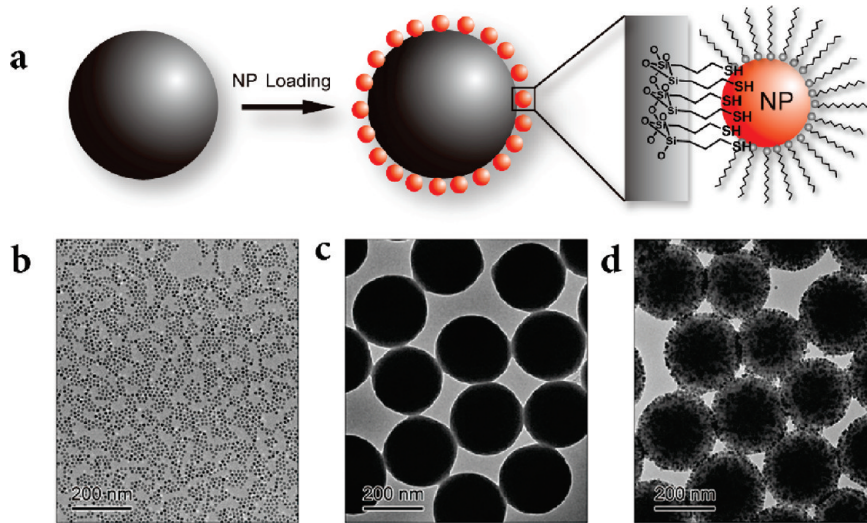


Figure 1. (a) Schematic illustration showing the procedure of self-assembly of hydrophobic nanoparticles on MPS spheres. (b) TEM images of oleic acid-capped $\gamma\text{-Fe}_2\text{O}_3$ nanoparticles, (c) MPS spheres, and (d) $\gamma\text{-Fe}_2\text{O}_3$ nanoparticles assembled on the surface of MPS spheres.

exchange processes usually involve several extra steps and in many cases are detrimental to the physical properties of the nanoparticles because the new hydrophilic ligands may not be able to effectively insulate the inorganic cores from the aqueous environment. For example, ligand exchange of hydrophobic trioctylphosphine oxide (TOPO) on the surface of CdSe/ZnS quantum dots (QDs) with various hydrophilic ligands causes a significant decrease in quantum efficiencies.^{28,30} Furthermore, the new ligands tend to desorb gradually from the nanoparticles, leading to aggregation and precipitation of the nanoparticles. More importantly, if more than one type of nanoparticles is needed for achieving multiple functions, each must be surface-treated separately before assembly. Therefore, it is highly desirable to develop a simple and general approach that allows the fabrication of multifunctional nanostructures by direct assembly of hydrophobic nanoparticles of various compositions. As their major applications are in the biomedical fields, it is also highly desired that these multifunctional systems be dispersible in water.

The strong coordinating interactions between alkanethiols and metal surfaces have been extensively studied and utilized in the formation of self-assembled monolayers (SAMs) on metal surfaces.³¹ It has also been reported that alkanethiols can adsorb onto metal oxide surfaces (such as TiO₂,³² ZnO,^{33,34} and SnO₂³⁵) and semiconductor substrates (such as InP,^{36,37} InAs,^{38,39} and GaAs,^{40,41} and metal sulfides⁴²). Recently, the thiol-metal interaction has been used to immobilize nanoparticles on alkanethiol-modified solid substrates^{43–46} and has been further extended to the colloidal substrates by assembling Au nanoparticles to thiol-functionalized silica colloids.^{47,48} Philipse et al. have explored the attachment of magnetic particles to colloidal silica that was grafted with (3-mercaptopropyl)trimethoxysilane (MPS).^{49,50} Their efforts, however, have been still limited to only water-soluble $\gamma\text{-Fe}_2\text{O}_3$ and CoFe₂O₄ nanoparticles, probably due to the low density of thiol groups achievable during the surface modification of colloidal silica. Our prior studies have shown that colloidal silica with a high surface loading of thiol groups can effectively harvest hydrophobic Au nanocrystals from nonpolar solutions.⁵¹

In this Letter, we explore the use of thiol-terminated colloidal organosilica (mercapto-silica) particles to directly immobilize various types of hydrophobic ligand-capped nanoparticles and

further develop a general and powerful self-assembly method for the fabrication of multifunctional composite nanostructures. Briefly, mercapto-silica colloidal particles made from MPS are first synthesized as adsorbent hosts, named as MPS spheres. Nanoparticles of desired functions are synthesized separately using well-established thermolysis methods, and then efficiently immobilized on the surface of MPS spheres by taking advantage of the high density thiol groups. In order to improve the chemical/mechanical stability and water-dispersibility, the composites can be further coated with a thin shell of normal silica. After demonstrating this simple assembly process, we generalize the procedure by immobilizing nanoparticles on mercapto-silica modified nanoscale objects, thus opening the door to the fabrication of more complex multifunctional composite structures.

Figure 1a outlines the general self-assembly strategy for the fabrication of monodisperse, well-defined nanoparticle-silica multifunctional composites. The assembly involves two essential building blocks: mercapto-silica spheres and hydrophobic ligand-capped nanoparticles. In a typical process, MPS precursor is hydrolyzed rapidly in an ammonia solution to yield spherical colloids.^{51–53} These mercapto-silica spheres are both structurally and functionally different from normal silica particles prepared from alkoxide precursors such as tetraethyl orthosilicate (TEOS). The use of MPS grants the resulting spheres a layer of high density surface thiol groups, which are expected to tether a dense layer of nanoparticles through the strong thiol-metal interactions. On the other hand, the abundant mercaptopropyl groups make the MPS spheres dispersible in nonpolar solvents such as toluene, facilitating the approaching of mercapto-silica and hydrophobic nanocrystals during the assembly process. The narrowly distributed MPS spheres with controlled sizes ranging from ~ 150 nm to $\sim 3.5 \mu\text{m}$ can be produced by simply changing the reaction conditions, for example, the amount of the silane precursor,⁵³ making it possible to produce uniform multifunctional nanocomposites with the desired dimensions. Hydrophobic ligand-capped nanoparticles are prepared through standard high-temperature thermolysis reaction.^{24–26,28} Figure 1b,c shows typical transmission electron microscopy (TEM) images of oleic acid-capped $\gamma\text{-Fe}_2\text{O}_3$ nanoparticles (diameter, 12 ± 0.7 nm) and MPS spheres (diameter, 280 ± 30 nm).

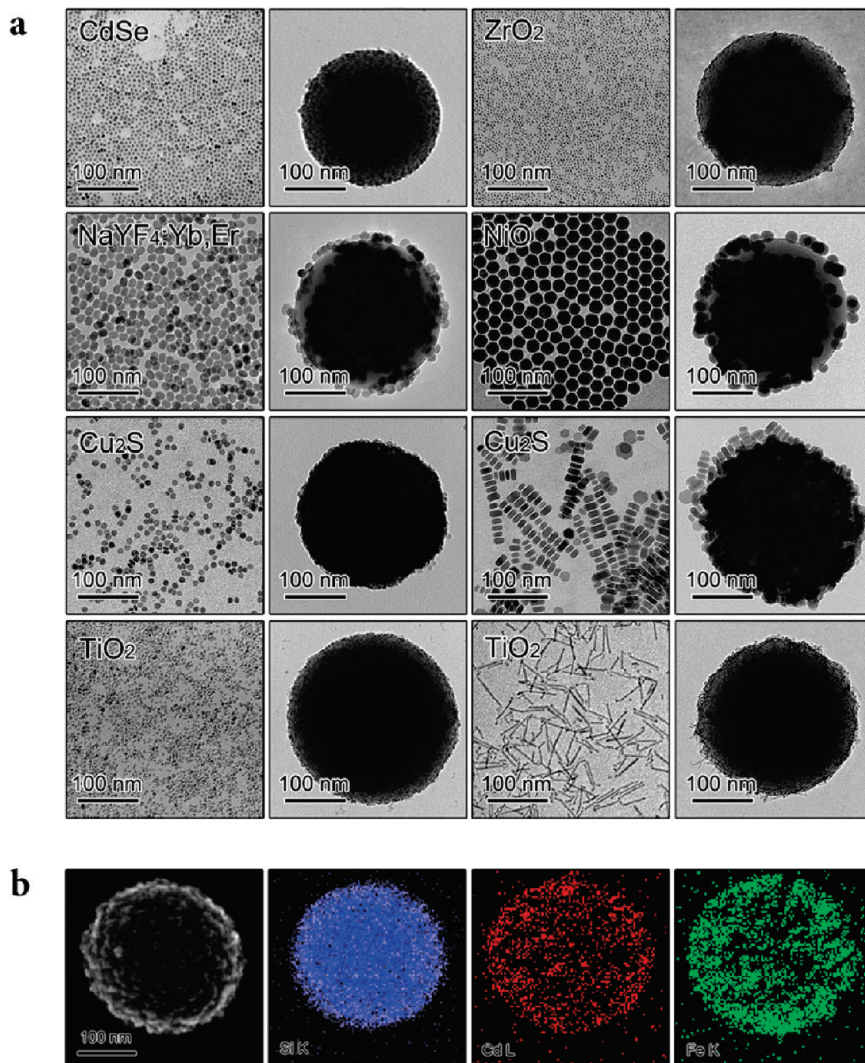


Figure 2. (a) TEM images of various hydrophobic nanoparticles assembled on the surface of MPS spheres: left columns (column 1 and 3) show the different nanoparticles and right columns (column 2 and 4) represent the corresponding nanoparticle-capped MPS spheres. The ZrO₂, TiO₂ nanodots are originally protected by TOPO, NaYF₄:Yb,Er, TiO₂ nanorods by oleic acid, CdSe and NiO by TOPO and oleylamine, and both small and large Cu₂S nanodisks by 1-dodecanethiol. (b) SEM image and the corresponding EDX mapping of the elemental distribution of Si, Cd, and Fe in a composite sphere of MPS@ γ -Fe₂O₃&CdSe.

Nanoparticles are assembled on the surface of MPS spheres by simply mixing them in nonpolar solvents such as toluene and cyclohexane. Generally, excess nanoparticles are used to ensure the dense coverage on the MPS spheres. Nanoparticle-capped MPS spheres are collected after washing several times with nonpolar solvent to remove free nanoparticles. As shown in Figure 1d, a monolayer of γ -Fe₂O₃ nanoparticles can be clearly observed on the originally smooth surface of MPS spheres. No free nanoparticles can be observed, suggesting a strong attraction between the nanoparticles and MPS spheres. It is believed that during the assembly process, the thiol groups can partially replace the original surface ligands (oleic acid) and coordinate to the metal sites on the nanoparticle surface.

Thiols form stable bonds with most metal cations except alkali and alkaline earth ions.⁸ To test the versatility of the assembly process, various hydrophobic metal compound nanoparticles including trioctylphosphine oxide (TOPO) and oleylamine-capped CdSe,⁵⁴ TOPO-capped ZrO₂,⁵⁵ oleic acid-capped NaYF₄:Yb,Er,⁵⁶

TOPO-and oleylamine-capped NiO,⁵⁷ 1-dodecanethiol-capped Cu₂S discs,⁵⁸ TOPO-capped TiO₂ dots⁵⁹ and oleic acid-capped rods⁶⁰ were assembled on the surface of the MPS spheres, as shown in Figure 2a. A layer of nanoparticles can be easily identified on the surface of each MPS sphere, indicating the generality of the assembly strategy for hydrophobic metal compound nanoparticles. Note that Cu₂S discs with different diameters (8 and 20 nm) show a similar high affinity for the MPS spheres, indicating a minimal size effect on the binding process. This has been also confirmed by the dense coverage of γ -Fe₂O₃ nanoparticles of 5, 12, and 20 nm on MPS spheres. The similar adsorption behavior of TiO₂ nanodots and nanorods on MPS spheres also suggests that the shape of nanoparticles has no significant effect on assembly efficiency.

The simple assembly process allows great flexibility in incorporating multiple nanoparticle components. A competition for immobilization on the surface of MPS spheres would appear among various types of nanoparticles due to their different affinity to thiol groups, which generally follows the Hard Soft

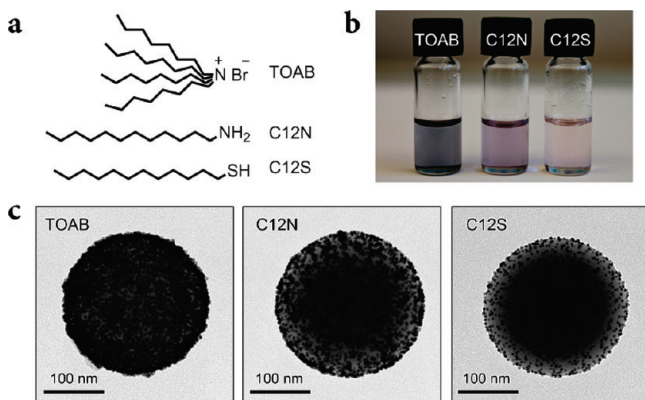


Figure 3. Effect of original capping ligands on nanoparticle assembly. (a) Molecular structures of the three protection ligands capped on Au nanoparticles (TOAB, C12N and C12S). (b) Digital photo of toluene dispersion of MPS spheres loaded with Au nanoparticles whose surfaces are capped with the three different protection ligands. (c) TEM images of the corresponding MPS spheres in panel b.

Acid Base (HSAB) theory. Nanoparticles containing soft-acid cations such as Pt(II), Cu(I), Cd(II) and Au(I) bind to thiol groups much more strongly compared with those made of hard-acid cations such as Fe(III) and Ti(IV). In a nanoparticle mixture, it is necessary to increase the relative concentration of those with low-affinity to ensure sufficient loading. As an example shown in Figure 2b, we demonstrate here the assembly of γ -Fe₂O₃ nanoparticles and CdSe QDs on MPS spheres by mixing their dispersions at a particle number ratio of 10:1. The simultaneous capture of nanoparticles of γ -Fe₂O₃ and QD on the MPS surfaces has been confirmed by using scanning electron microscopy (SEM) imaging and energy dispersive X-ray (EDX) elemental mapping of a typical composite sphere. The strong Si signal across the sphere confirms the organosilica core, while the Fe and Cd signals both detected in the surface region clearly suggests the coadsorption of these two types of particles.

In order to reach the metal sites on the nanoparticle surface, the thiol groups of MPS spheres may partially replace the original capping ligands on the nanoparticle surface. To evaluate this ligand replacement, hydrophobic Au nanoparticles capped with three different protection ligands, tetraoctylammonium bromide (TOAB), dodecylamine (C12N), and 1-dodecanethiol (C12S) are used for assembly.⁵¹ The molecular structures of these ligands are shown in Figure 3a. After mixing with Au nanoparticles in toluene for \sim 20 min, the MPS spheres were separated from the mixture and washed a few times to remove free Au nanoparticles. Figure 3b presents the digital photos of toluene dispersions of Au nanoparticle-immobilized MPS spheres with TOAB-, C12N-, and C12S-capped spheres exhibiting blue, purple, and light red colors, respectively. The shift of the surface plasmon resonance bands (color change) is the result of interparticle electromagnetic coupling: MPS spheres attract more TOAB-capped Au nanoparticles, resulting in smaller interparticle distance and consequently a larger blue shift.⁵¹ The color intensity also indicates the loading of nanoparticles on MPS spheres. Because of the stability order of bonding Au-TOAB < Au-C12N < Au-C12S, the weaker capping ligands are believed to detach easily from the Au surface to allow for the formation of Au-S bonds, leading to higher nanoparticle loading, as confirmed in Figure 3c. The interesting fact that some C12S-capped Au nanoparticles can still be captured by MPS spheres indicates that the thiol

groups on MPS spheres can still replace some of the original alkanethiols to form new Au-S bonds even though the new bonds are similar to the original bonds in strength. This is consistent with our understanding of the dynamic nature of the ligand adsorption on nanoparticle surface.²⁴ As ligand replacement will eventually reach dynamic equilibrium, we predict that nanoparticle immobilization can always occur even if the new thiol-nanoparticle bond is weak compared to the original ligand-nanoparticle interaction, but the actual loading may be significantly affected by the relative bond strength.

The loading density of nanoparticles on the MPS spheres is related to their number ratio during assembly. If we assume the nanoparticles on the MPS spheres arrange in a hexagonal close-packing structure, the number of nanoparticles per MPS sphere, N , can be estimated by $N = 4\alpha(1 + R/r)^2$, where $\alpha = 0.906$ is the density of the circular hexagonal arrangement, and R and r are the radii of MPS spheres and nanoparticles, respectively. This equation allows us to estimate the amount of nanoparticles that is needed for a required loading density, for example, one MPS sphere with diameter of 300 nm can immobilize $\sim 5 \times 10^3$ 8-nm nanoparticles. Experimentally, we can quantify the nanoparticle loading by measuring their optical absorption or photoluminescence (PL), as shown in Figure 4a by using CdSe/CdZnS QDs as an example.⁶¹ QDs \sim 8 nm in diameter in a toluene solution ($500 \mu\text{L}$, $\sim 10^{14}$ particles per mL) were mixed with different amounts of MPS sphere solution ($\sim 2 \times 10^{10}$ spheres per mL) for 1 h under vigorous shaking, followed by centrifugation at 11000 rpm for 10 min (free QDs remain in supernatant at this speed). Supernatant was collected for fluorescence measurement to monitor the amount of the free QDs left in the solution, and the precipitates were harvested for qualitative analysis of QD loading using TEM. As shown in Figure 4b, the fluorescence intensity of the supernatant decreased as more MPS solution was added to the system. When only a small amount of MPS solution ($< 100 \mu\text{L}$) was added, QDs remained in excess so that the decrease in fluorescence was nearly proportional to the added amount of MPS solution. The corresponding TEM image (Figure 4c) confirms that the surface of every MPS sphere is fully occupied by QDs. Adding more MPS spheres (200 and $300 \mu\text{L}$) led to a decrease in fluorescence intensity because more QDs were captured by MPS spheres and then removed from the supernatant. No free QDs were left in the supernatant when $300 \mu\text{L}$ of MPS spheres was added. At this stage there are not enough QDs to cover all the MPS surfaces in the form of a close-packed monolayer, as indicated in the TEM image in Figure 4c. When $500 \mu\text{L}$ of MPS solution was added, even fewer QDs were adsorbed on each MPS sphere. If we assume that $200 \mu\text{L}$ of MPS solution is the amount needed for a close-packed monolayer of QDs, each MPS sphere can capture 10^4 QDs as estimated from the concentration and volume of MPS spheres and QDs that are used. This value is consistent with the result calculated based on geometric considerations (5×10^3).

The adsorption of hydrophobic nanoparticles onto MPS spheres results in composite particles that are nondispersible in water, thus preventing their direct application in environmental and biomedical applications. This limitation can be conveniently addressed by overcoating the composite particles with an additional layer of normal silica. Silica coating can endow the composites with biocompatibility and the possibility of subsequent functionalization. The additional advantages of using silica as a coating material mainly lie in its chemical stability, easy regulation of the coating process, controllable porosity, processability, and optical transparency.⁶²

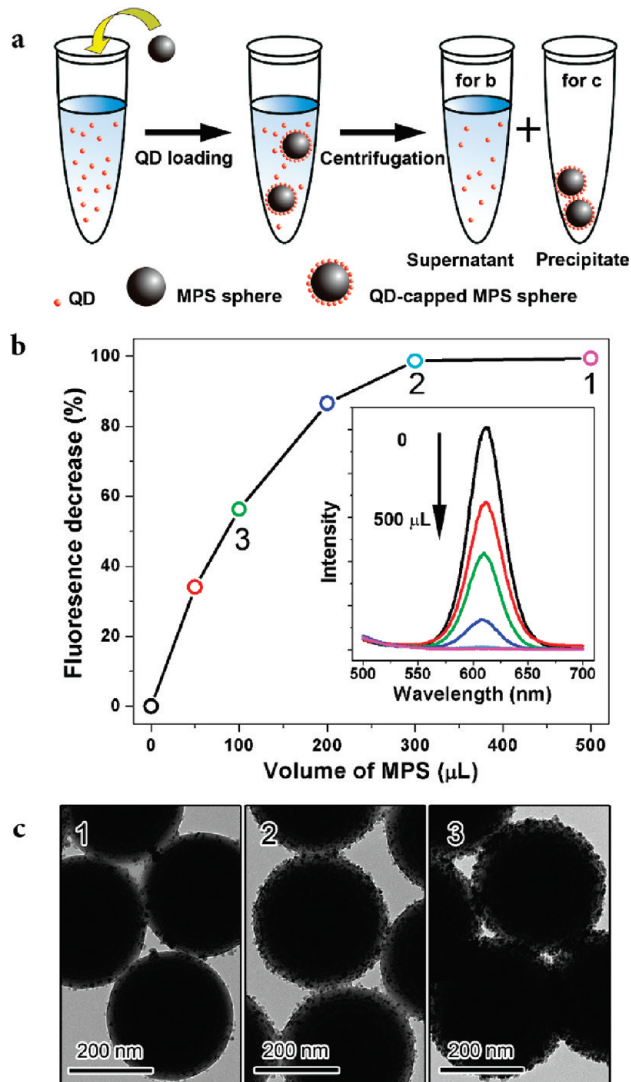


Figure 4. (a) Schematic diagram of the self-assembly of CdSe@CdZnS QDs on MPS spheres, showing how the PL spectra in (b) and TEM images in (c) were recorded. The original surface of QDs was covered by oleic acid. (b) PL spectra of the supernatant after adsorption of QDs by different amount of MPS spheres. (c) TEM images of the precipitates (QD-capped MPS spheres) corresponding to the three points highlighted with numbers 1, 2, and 3 in Figure b.

The nanoparticle-capped MPS composites are first transferred to aqueous phase by using additional surfactants to adsorb onto the surface of composite spheres through the formation of bilayer structures, as illustrated in Figure 5a. The phase transfer makes it convenient to subsequently grow a silica layer using the well-known Stöber method.⁶³ The formation of a bilayer through hydrophobic–hydrophobic interaction also helps preserve the original ligands on the nanocrystal surface. As an example, we use an anionic surfactant, sodium dodecyl sulfate (SDS), to mediate the silica coating of oleic acid-capped MPS@ γ -Fe₂O₃ composite spheres. After SDS adsorption, the MPS@ γ -Fe₂O₃ composites were transferred into an ammonia/water/ethanol mixture and directly coated with uniform silica shells upon careful addition of TEOS. Figure 5b displays typical images of SiO₂ overcoated MPS@ γ -Fe₂O₃ spheres. The thickness of the silica shell can be tuned from ten to several hundred nanometers by simply

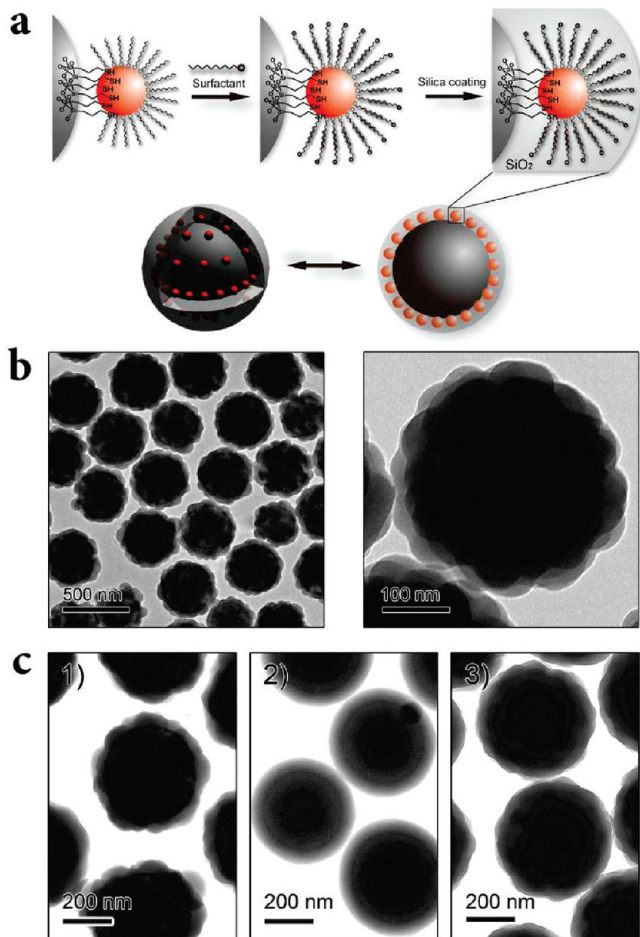


Figure 5. (a) Schematic illustration showing the approach for transferring nanoparticle-capped MPS spheres from oil to water phase by forming bilayer structure and subsequent silica coating. (b) TEM images of low and high magnification of silica coated γ -Fe₂O₃ nanoparticle-capped MPS spheres ($\text{MPS}@\gamma\text{-Fe}_2\text{O}_3@\text{SiO}_2$) synthesized in the presence of SDS. The γ -Fe₂O₃ nanoparticles were originally protected by oleic acid. (c) TEM images of MPS spheres capped with various nanoparticles and then surface coated with silica in the presence of SDS surfactant: (1) $\text{MPS}@\text{Au}@\text{SiO}_2$, (2) $\text{MPS}@\text{TiO}_2$ nanorods@ SiO_2 , and (3) $\text{MPS}@\text{ZrO}_2$ @ SiO_2 . The Au nanoparticles were originally protected by dodecylamine (C12N), TiO₂ nanorods by oleic acid, and ZrO₂ nanodots by TOPO.

changing the amount of TEOS precursor. Interestingly, silica seems to initially nucleate on the individual nanoparticle surface and then grow independently before they eventually merge into a single layer. As a result, the silica coating possesses a rough surface until it reaches a thickness of \sim 100 nm. SDS has been demonstrated to be very effective in assisting the silica coating of composite spheres capped with various nanoparticles. This silica coating method assisted by SDS surfactant is universal for other hydrophobic nanoparticles-capped MPS spheres. In fact, the process has little to do with the compositions of nanoparticles and can be applied to passivate various nanoparticle/MPS systems as long as the additional surfactants can disperse these nanoparticles in the mixture of ethanol/H₂O/NH₃, which is the chemical environment required for the Stöber method for silica coating. Figure 5c demonstrates a few more examples of normal silica passivated MPS@nanoparticle assemblies with the nanoparticles being Au dots, TiO₂ rods, and ZrO₂ dots. Because of their

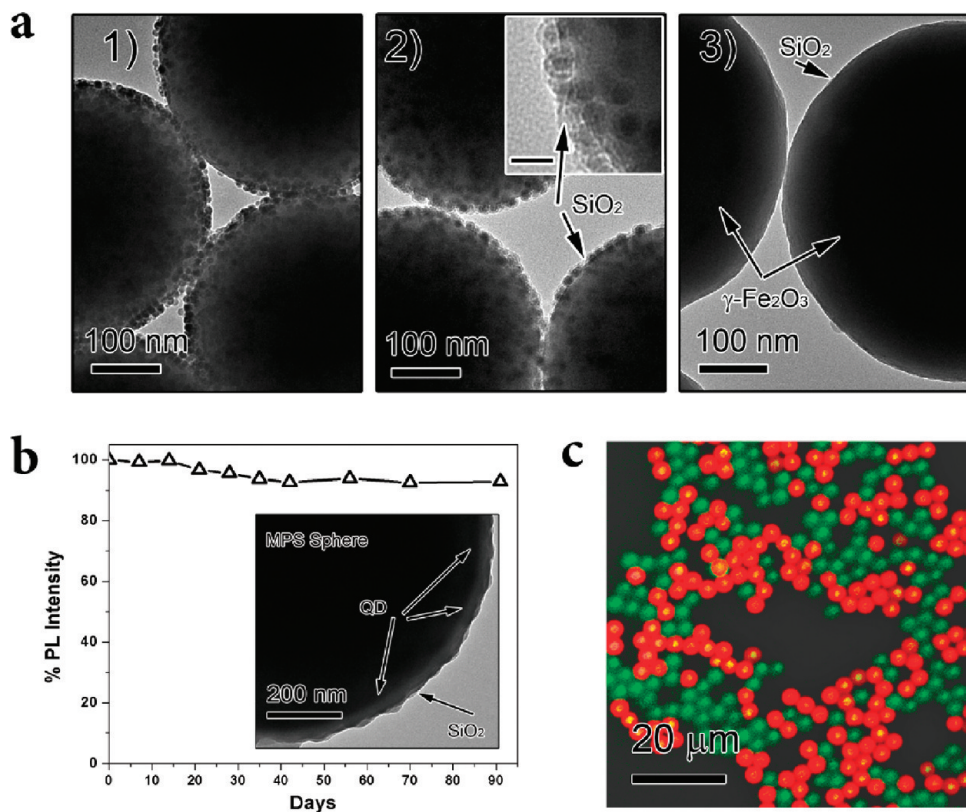


Figure 6. (a) TEM images of of $\gamma\text{-Fe}_2\text{O}_3$ nanoparticle-capped MPS spheres prepared in the presence of CTAB: (1) before silica coating; (2) after SiO₂ coating with CTAB as the surfactant in aqueous NaOH solution; (3) after additional SiO₂ coating using the standard Stöber process. The $\gamma\text{-Fe}_2\text{O}_3$ nanoparticles were originally protected by oleic acid. Inset in (2) is the corresponding TEM image at high magnification showing the presence of a thin silica layer (scale bar: 20 nm). (b) PL intensity as a function of time after storing the MPS@QD@SiO₂ composite spheres in water under ambient conditions; inset is the TEM image of a portion of a typical MPS@QD@SiO₂ sphere. The surface of CdSe@CdZnS QDs was originally covered by oleic acid. (c) Confocal optical microscopy image of 3.5 μm MPS spheres loaded with QDs of two different sizes. QDs of different colors were assembled on MPS spheres separately and then mixed together for imaging. The sample was excited with a focused 488 nm line of Ar⁺ laser.

small size compared to that of the MPS spheres, the nanoparticles cannot be individually identified in the TEM images and only a dark ring can be observed within the silica coating. Other typical surfactants, such as CTAB, can also be used to mediate silica coating on composite spheres. As shown in Figure 6a with MPS@ $\gamma\text{-Fe}_2\text{O}_3$ as an example, we adapted a previously reported method to first deposit a thin silica coating of a few nanometers on the composite surface by hydrolyzing TEOS in aqueous solution of CTAB with dilute NaOH solution as catalyst.⁶⁴ The thickness of the silica layer can be further increased by an additional step of standard Stöber process. Unlike the case using SDS, this two step procedure produces a very smooth silica surface even at a relatively small thickness. This procedure is especially useful for coating TOPO-capped MPS@QD spheres because CTAB causes smaller disturbance to the luminescence of QDs than SDS. Figure 6b demonstrates the high stability of the PL of MPS@QD@SiO₂ composites with the TEM image of a portion of a typical sphere shown in the inset. The decrease of PL intensity is only about 10% even after 3 months of storage in water, which is significantly better than that of typical ligand-exchanged QDs. Surface passivation provided by silica and the intact ligand protection are believed to be the two main reasons for this excellent optical stability. Figure 6c shows a multicolor fluorescence microscopy image of a mixture of two types of “monochromatic” MPS@QD@SiO₂ spheres with an average diameter of 3.5 μm . These green and red spheres were prepared separately by using single-color quantum dots with emission wavelengths at 545 and 610 nm, respectively, and then

mixed and imaged under a single wavelength light. All the spheres are observed with clearly distinguishable emission colors.

The necessity of MPS for high density thiol groups may appear as a limitation because MPS has only been produced in the form of microspheres and the functional nanoparticles can only be attached to the external surface of the spheres in the form of a monolayer. On the other hand, normal colloidal silica is well-known for its ability to form a conformal coating on various nanostructures with a high degree of control over the thickness. Here we generalize the assembly process by coating mercapto-silica onto the surface of other nanoscale objects so that further nanoparticle assembly can occur on hosts with more complex morphologies than spheres. Our strategy is to first coat nano-objects such as dots, rods and wires with normal silica, and then introduce mercapto-silica to the surface through a co-condensation method. In the second step, multiple injections of the precursors were applied. The ratio of MPS to TEOS gradually increased for every injection to ensure a high density of thiol groups on the surface. The thiol-functionalized layer had been characterized by FTIR spectroscopy. After coating the normal silica spheres with an MPS layer, two bands in the ranges of 2950–2850 and 2600–2500 cm^{-1} appeared, which can be attributed to the C–H and S–H stretching of the attached propanethiol groups.⁶⁵ The relatively strong absorption of C–H and S–H stretching in the IR spectrum indicates that the loading of thiol groups is significantly higher than that of colloidal silica

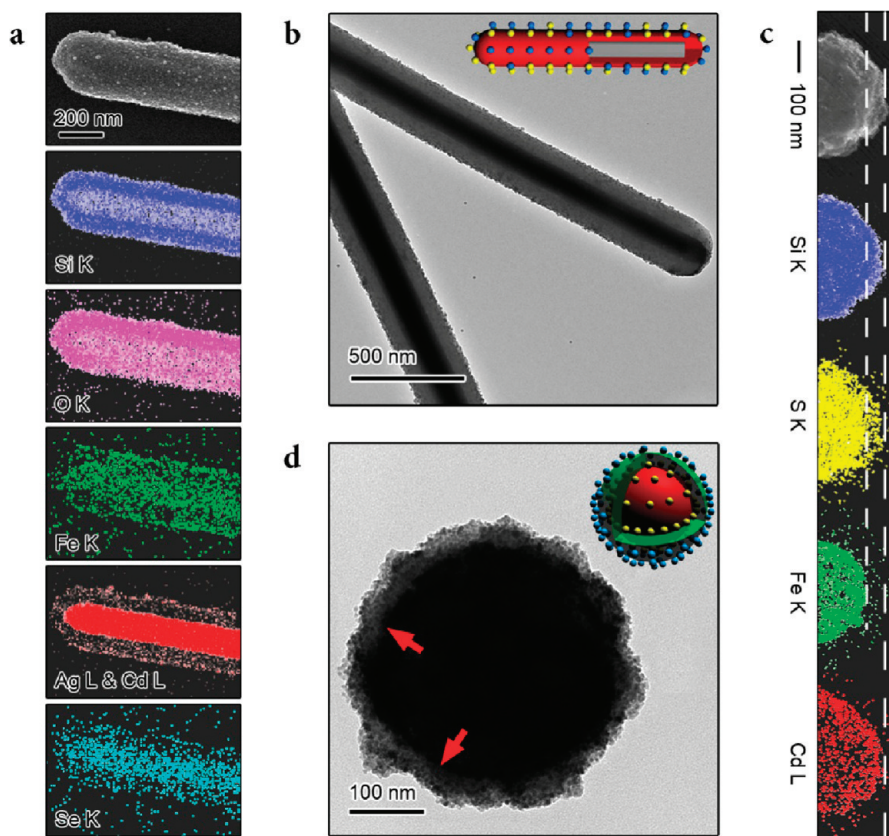


Figure 7. (a,b) SEM image and EDX mapping (a) and TEM image (b) of the elemental distribution of Ag nanowire@SiO₂&MPS@CdSe&γ-Fe₂O₃ composite nanowires. The Ag nanowires were synthesized by using a polyol process in the presence of poly(vinyl pyrrolidone) (PVP), surface coated with normal silica using the Stöber process, modified with MPS layer, and then decorated with TOPO/oleylamine-capped CdSe and oleic acid-capped γ-Fe₂O₃ nanoparticles. (c,d) SEM images and EDX mapping of the elemental distribution (c) and TEM image (d) of a MPS@γ-Fe₂O₃@SiO₂&MPS@CdSe multilayer composite, synthesized by sequential procedures including initial loading of oleic acid-capped γ-Fe₂O₃ nanoparticles on MPS spheres, surface coated with normal silica using the Stöber process, modified with MPS layer, and then decorated with TOPO/oleylamine-capped CdSe nanoparticles. Insets in (b) and (d) are schematic illustrations of the assembled structures.

spheres modified with MPS silane using conventional grafting methods (where only a submonolayer of MPS can be attached).

The ability to form MPS coatings on normal silica surfaces opens the door to the fabrication of a large variety of multi-functional composite nanostructures. Functional materials can now be incorporated as cores inside normal silica, whose surface can be modified with high density thiol groups for attaching other types of functional nanoparticles. Here, we have demonstrated a Fe₃O₄@SiO₂&MPS@QD@SiO₂ multilayer structure by using the simple solution phase assembly processes. First, superparamagnetic Fe₃O₄ particles with a diameter of ~100 nm were coated with SiO₂. After coating with a MPS layer, QDs were assembled on the surface, and subsequently another layer of SiO₂ was coated to make the composites water dispersible. The product exhibits strong fluorescence under UV excitation and superparamagnetic property that allows fast magnetic separation using an external magnet.

The process also allows the functionalization of nonspherical objects. As a demonstration, we have prepared Ag@SiO₂&MPS@γ-Fe₂O₃&QD multilayer composite nanowires by using this simple assembly processes. Silver nanowires were synthesized using a polyol process, coated with normal silica,⁶⁶ modified with MPS, and surface-immobilized with mixed nanoparticles of γ-Fe₂O₃ and QDs. Figure 7a shows the elemental distribution of Si, O, Fe, Ag, Cd, and Se, as analyzed by EDX mapping. Ag@SiO₂ cable-like structure

can be easily identified by the strong Ag signal at the core and Si, O signals at the shell regions. The weaker but evenly distributed signals from Fe, Cd, and Se prove the thin layer of immobilized γ-Fe₂O₃ and QDs. The uniform attachment of nanoparticles can be also clearly observed in the TEM image in Figure 7b. The successful expansion to nonspherical morphologies makes this assembly process truly unique in comparison to conventional methods.

Analogous to the LbL approach,^{17,18,67} the assembly process here also allows multilayer assembly by repeating the nanoparticle immobilization, silica coating, and MPS modification procedures. As a demonstration, we started with MPS spheres (~300 nm in diameter), immobilized γ-Fe₂O₃ nanoparticles on the surface, overcoated with a thin SiO₂/MPS layer, and immobilized QDs on the surface again. Figure 7c,d shows the EDX elemental mapping and a typical TEM image of a multilayer MPS@γ-Fe₂O₃@SiO₂&MPS@QD structure. The dark ring marked with arrows is the layer of γ-Fe₂O₃ nanoparticles. The gray area outside this ring is the SiO₂&MPS layer with thickness of ~50 nm. QDs can be clearly seen on the sphere surface. As indicated by the two dotted lines in Figure 7c, the different locations of Fe and Cd (150 nm for Fe, 200 nm for Cd from the sphere's center) clearly suggests that the γ-Fe₂O₃ nanoparticles and QDs are distributed within different layers of the composite. The gap between these two nanoparticle layers is 50 nm which corresponds to the thickness of SiO₂&MPS layer.

Interestingly, a strong S signal is also observed in this gap, indicating high loading of thiol groups in this layer. All these observations confirm the complex structure with multiple types of nanoparticles positioned at different layers. This multilayer assembly strategy not only provides the means to improve the loading capacity but also makes it convenient to increase the number of functions while maintaining the loading density of each component.

In summary, we have developed a general process that allows convenient production of multifunctional colloidal particles by direct self-assembly of hydrophobic nanoparticles on host nanostructures containing mercapto-silica surfaces. The resulting composite structures can be further conveniently overcoated with a layer of normal silica to stabilize the assemblies and render them highly dispersible in water for biomedical applications. As the entire fabrication process does not involve complicated surface modification procedures, the hydrophobic ligands on the nanoparticles are not disturbed significantly so that they retain their original properties such as highly efficient luminescence. Many complex composite nanostructures with tailored functions can be conveniently produced by assembling nanoparticles of various compositions, sizes, and morphologies. Although our focus here has been on the immobilization of hydrophobic nanoparticles as this has been a major challenge in the field, the developed process can be easily extended to the assembly of hydrophilic nanoparticles with minimal modifications. This universal, highly configurable, scalable and reproducible assembly process will help to produce various multifunctional structures for many important technological applications. Furthermore, nanoparticles of different compositions are expected to have different releasing behaviors depending on the strength of the specific nanoparticle–thiol interaction, thus promising for controlled drug delivery or related applications.

■ ASSOCIATED CONTENT

S Supporting Information. Detailed synthesis recipes, additional TEM images of various MPS@NP composite spheres and silica passivated assemblies, FTIR spectra showing MPS coating, results demonstrating MPS@Au& γ -Fe₂O₃@SiO₂ composite structures as magnetically recoverable catalysts, and TEM images showing the assembly of hydrophilic nanoparticles. This material is available free of charge via the Internet at <http://pubs.acs.org>.

■ AUTHOR INFORMATION

Corresponding Author

*E-mail: yadong.yin@ucr.edu.

■ ACKNOWLEDGMENT

This work has been supported in part by the U.S. Department of Energy (Grant DE-SC0002247) and a Faculty Early Career Development (CAREER) award from the National Science Foundation (DMR-0956081). Y.Y. also thanks the Research Corporation for Science Advancement for the Cottrell Scholar Award, 3M for the Nontenured Faculty Grant, and DuPont for the Young Professor Grant. Part of TEM work was performed at ORNL's Shared Research Equipment (SHaRE) User Facility, which is sponsored by the Office of Basic Energy Sciences, U.S. DOE.

■ REFERENCES

- (1) Jun, Y.-W.; Lee, J.-H.; Cheon, J. *Angew. Chem., Int. Ed.* **2008**, *47*, 5122.
- (2) Kim, J. S.; Rieter, W. J.; Taylor, K. M. L.; An, H.; Lin, W.; Lin, W. *J. Am. Chem. Soc.* **2007**, *129*, 8962.
- (3) Salgueirino-Maceira, V.; Correa-Duarte, M. A. *Adv. Mater.* **2007**, *19*, 4131.
- (4) Suh, W. H.; Suh, Y.-H.; Stucky, G. D. *Nano Today* **2009**, *4*, 27.
- (5) Liang, M.; Lu, J.; Kovochich, M.; Xia, T.; Ruehm, S. G.; Nel, A. E.; Tamanoi, F.; Zink, J. I. *ACS Nano* **2008**, *2*, 889.
- (6) Sathe, T. R.; Agrawal, A.; Nie, S. M. *Anal. Chem.* **2006**, *78*, 5627.
- (7) Koole, R.; Mulder, W. J. M.; van Schooneveld, M. M.; Strijkers, G. J.; Meijerink, A.; Nicolay, K. *Wiley Interdiscip. Rev.: Nanomed. Nanobiotechnol.* **2009**, *1*, 475.
- (8) Selvan, S. T.; Patra, P. K.; Ang, C. Y.; Ying, J. Y. *Angew. Chem., Int. Ed.* **2007**, *46*, 2448.
- (9) Kim, J.; Lee, J. E.; Lee, J.; Yu, J. H.; Kim, B. C.; An, K.; Hwang, Y.; Shin, C.-H.; Park, J.-G.; Kim, J.; Hyeon, T. *J. Am. Chem. Soc.* **2006**, *128*, 688.
- (10) Wilson, R.; Spiller, D. G.; Prior, I. A.; Veltkamp, K. J.; Hutchinson, A. *ACS Nano* **2007**, *1*, 487.
- (11) Kim, J.; Park, S.; Lee, J. E.; Jin, S. M.; Lee, J. H.; Lee, I. S.; Yang, I.; Kim, J.-S.; Kim, S. K.; Cho, M.-H.; Hyeon, T. *Angew. Chem., Int. Ed.* **2006**, *45*, 7754.
- (12) Spasova, M.; Salgueirino-Maceira, V.; Schlachter, A.; Hilgendorff, M.; Giersig, M.; Liz-Marzan, L. M.; Farle, M. *J. Mater. Chem.* **2005**, *15*, 2095.
- (13) Shylesh, S.; Schuenemann, V.; Thiel, W. R. *Angew. Chem., Int. Ed.* **2010**, *49*, 3428.
- (14) Ge, J.; Zhang, Q.; Zhang, T.; Yin, Y. *Angew. Chem., Int. Ed.* **2008**, *47*, 8924.
- (15) Xuan, S.; Wang, Y.-X. J.; Yu, J. C.; Leung, K. C.-F. *Langmuir* **2009**, *25*, 11835.
- (16) Lee, K. S.; Woo, M. H.; Kim, H. S.; Lee, E. Y.; Lee, I. S. *Chem. Commun.* **2009**, 3780.
- (17) Kotov, N. A.; Dekany, I.; Fendler, J. H. *J. Phys. Chem.* **1995**, *99*, 13065.
- (18) Caruso, F.; Susha, A. S.; Giersig, M.; Mohwald, H. *Adv. Mater.* **1999**, *11*, 950.
- (19) Stoeva, S. I.; Huo, F.; Lee, J.-S.; Mirkin, C. A. *J. Am. Chem. Soc.* **2005**, *127*, 15362.
- (20) Wang, Z.; Zhao, Z.; Zhang, J.; Li, Z.; Gao, Y.; Wang, C.; Zhang, H.; Yang, B. *J. Colloid Interface Sci.* **2009**, *339*, 83.
- (21) Lee, J.-H.; Jun, Y.-w.; Yeon, S.-I.; Shin, J.-S.; Cheon, J. *Angew. Chem., Int. Ed.* **2006**, *45*, 8160.
- (22) Wang, C. G.; Chen, J.; Talavage, T.; Irudayaraj, J. *Angew. Chem., Int. Ed.* **2009**, *48*, 2759.
- (23) Sun, S.; Zeng, H.; Robinson, D. B.; Raoux, S.; Rice, P. M.; Wang, S. X.; Li, G. *J. Am. Chem. Soc.* **2004**, *126*, 273.
- (24) Yin, Y.; Alivisatos, A. P. *Nature* **2005**, *437*, 664.
- (25) Murray, C. B.; Norris, D. J.; Bawendi, M. G. *J. Am. Chem. Soc.* **1993**, *115*, 8706.
- (26) Park, J.; An, K.; Hwang, Y.; Park, J.-G.; Noh, H.-J.; Kim, J.-Y.; Park, J.-H.; Hwang, N.-M.; Hyeon, T. *Nat. Mater.* **2004**, *3*, 891.
- (27) Talapin, D. V.; Rogach, A. L.; Kornowski, A.; Haase, M.; Weller, H. *Nano Lett.* **2001**, *1*, 207.
- (28) Bruchez, M., Jr.; Moronne, M.; Gin, P.; Weiss, S.; Alivisatos, A. P. *Science* **1998**, *281*, 2013.
- (29) Chan, W. C. W.; Nie, S. *Science* **1998**, *281*, 2016.
- (30) Talapin, D. V.; Rogach, A. L.; Mekis, I.; Haubold, S.; Kornowski, A.; Haase, M.; Weller, H. *Colloids Surf, A* **2002**, *202*, 145.
- (31) Schreiber, F. *Prog. Surf. Sci.* **2000**, *65*, 151.
- (32) Liu, G.; Rodriguez, J. A.; Chang, Z.; Hrbek, J.; Gonzalez, L. *J. Phys. Chem. B* **2002**, *106*, 9883.
- (33) Perkins, C. L. *J. Phys. Chem. C* **2009**, *113*, 18276.
- (34) Sadik, P. W.; Pearton, S. J.; Norton, D. P.; Lambers, E.; Ren, F. *J. Appl. Phys.* **2007**, *101*, 104514.
- (35) Liu, F.; Quan, B.; Liu, Z.; Chen, L. *Mater. Chem. Phys.* **2005**, *93*, 301.
- (36) Lim, H.; Carraro, C.; Maboudian, R.; Pruessner, M. W.; Ghodssi, R. *Langmuir* **2003**, *20*, 743.
- (37) Yamamoto, H.; Butera, R. A.; Gu, Y.; Waldeck, D. H. *Langmuir* **1999**, *15*, 8640.

- (38) Petrovykh, D. Y.; Smith, J. C.; Clark, T. D.; Stine, R.; Baker, L. A.; Whitman, L. J. *Langmuir* **2009**, *25*, 12185.
- (39) Tanzer, T. A.; Bohn, P. W.; Roschchin, I. V.; Greene, L. H.; Klem, J. F. *Appl. Phys. Lett.* **1999**, *75*, 2794.
- (40) Voznyy, O.; Dubowski, J. J. *J. Phys. Chem. C* **2008**, *112*, 3726.
- (41) McGuiness, C. L.; Diehl, G. A.; Blasini, D.; Smilgies, D.-M.; Zhu, M.; Samarth, N.; Weidner, T.; Ballav, N.; Zharnikov, M.; Allara, D. L. *ACS Nano* **2010**, *4*, 3447.
- (42) Buckley, A. N.; Goh, S. W.; Lamb, R.; Fan, L.-J.; Yang, Y.-W. *ECS Trans.* **2006**, *2*, 107.
- (43) Hu, K.; Brust, M.; Bard, A. J. *Chem. Mater.* **1998**, *10*, 1160.
- (44) Colvin, V. L.; Goldstein, A. N.; Alivisatos, A. P. *J. Am. Chem. Soc.* **1992**, *114*, 5221.
- (45) Mann, J. R.; Watson, D. F. *Langmuir* **2007**, *23*, 10924.
- (46) Lee, Y. L.; Huang, B. M.; Chien, H. T. *Chem. Mater.* **2008**, *20*, 6903.
- (47) Nakamura, T.; Yamada, Y.; Yano, K. *J. Mater. Chem.* **2007**, *17*, 3726.
- (48) Westcott, S. L.; Oldenburg, S. J.; Lee, T. R.; Halas, N. J. *Langmuir* **1998**, *14*, 5396.
- (49) Claesson, E. M.; Philipse, A. P. *Langmuir* **2005**, *21*, 9412.
- (50) Claesson, E. M.; Philipse, A. P. *Colloids Surf., A* **2007**, *297*, 46.
- (51) Lu, Z. D.; Goebl, J.; Ge, J. P.; Yin, Y. D. *J. Mater. Chem.* **2009**, *19*, 4597.
- (52) Nakamura, M.; Ishimura, K. *J. Phys. Chem. C* **2007**, *111*, 18892.
- (53) Lu, Z.; Sun, L.; Nguyen, K.; Gao, C.; Yin, Y. *Langmuir* **2011**, *27*, 3372.
- (54) Peng, Z. A.; Peng, X. *J. Am. Chem. Soc.* **2002**, *124*, 3343.
- (55) Joo, J.; Yu, T.; Kim, Y. W.; Park, H. M.; Wu, F.; Zhang, J. Z.; Hyeon, T. *J. Am. Chem. Soc.* **2003**, *125*, 6553.
- (56) Li, Z. Q.; Zhang, Y.; Jiang, S. *Adv. Mater.* **2008**, *20*, 4765.
- (57) Park, J.; Kang, E.; Son, S. U.; Park, H. M.; Lee, M. K.; Kim, J.; Kim, K. W.; Noh, H. J.; Park, J. H.; Bae, C. J.; Park, J. G.; Hyeon, T. *Adv. Mater.* **2005**, *17*, 429.
- (58) Wang, Y.; Hu, Y.; Zhang, Q.; Ge, J.; Lu, Z.; Hou, Y.; Yin, Y. *Inorg. Chem.* **2010**, *49*, 6601.
- (59) Trentler, T. J.; Denler, T. E.; Bertone, J. F.; Agrawal, A.; Colvin, V. L. *J. Am. Chem. Soc.* **1999**, *121*, 1613.
- (60) Joo, J.; Kwon, S. G.; Yu, T.; Cho, M.; Lee, J.; Yoon, J.; Hyeon, T. *J. Phys. Chem. B* **2005**, *109*, 15297.
- (61) Carion, O.; Mahler, B.; Pons, T.; Dubertret, B. *Nat. Protoc.* **2007**, *2*, 2383.
- (62) Piao, Y.; Burns, A.; Kim, J.; Wiesner, U.; Hyeon, T. *Adv. Funct. Mater.* **2008**, *18*, 3745.
- (63) Stober, W.; Fink, A.; Bohn, E. *J. Colloid Interface Sci.* **1968**, *26*, 62.
- (64) Gorelikov, I.; Matsuura, N. *Nano Lett.* **2008**, *8*, 369.
- (65) Caregnato, P.; Forbes, M. D. E.; Soria, D. B.; Martire, D. O.; Gonzalez, M. C. *J. Phys. Chem. C* **2010**, *114*, 5080.
- (66) Yin, Y.; Lu, Y.; Sun, Y.; Xia, Y. *Nano Lett.* **2002**, *2*, 427.
- (67) Hong, X.; Li, J.; Wang, M.; Xu, J.; Guo, W.; Li, J.; Bai, Y.; Li, T. *Chem. Mater.* **2004**, *16*, 4022.